

Binary stars and the UVX in early type galaxies

Fabiola Hernández-Pérez^{1*} and Gustavo Bruzual²

¹*Centro de Investigaciones de Astronomía, CIDA, Av. Alberto Carnevali, Mérida, Venezuela. A.P. 264, C.P. 5101*

²*Centro de Radioastronomía y Astrofísica, CRyA, UNAM, Campus Morelia, Michoacán. México. A.P. 3-72, C.P.58089*

Accepted 0000 December 15. Received 0000 December 14; in original form 0000 October 11

ABSTRACT

We use the Hernández-Pérez & Bruzual HB13 stellar population synthesis models to study the rôle of interacting binary pairs as progenitors of EHB stars. We assemble a sample of 3417 Early Type Galaxies observed both in the optical (*SDSS-DR8*) and the UV (*GALEX-GR6*). The galaxies in our sample can be classified according to their position in the colour-colour diagram as UV weak or red sequence galaxies ($\sim 48\%$), UV strong or UVX galaxies ($\sim 9\%$), and recent star forming galaxies ($\sim 43\%$). Analysing this sample using the HB13 models for various choices of basic model parameters we conclude that: (a) The *UVr* colours of UV weak and UV strong galaxies are reproduced by the models as long as the fraction of binary stars is at least 15%. (b) Higher metallicity models ($Z = 0.02$ and $Z = 0.03$) reproduce the colours of UV weak and UV strong galaxies better than lower Z models. The $Z = 0.03$ model is slightly bluer than the $Z = 0.02$ model in the UV strong region, indicating a weak relationship between UVX and Z . (c) The strength of UVX increases with age in the model population. This is at variance with the results of other models that include binary stars as progenitors of EHB stars.

Key words: galaxies: elliptical and lenticular – ultraviolet: galaxies – stars : binaries – stars: horizontal branch

1 INTRODUCTION

The spectral energy distribution of many early type galaxies (ETGs) and spiral galaxy bulges increases to shorter wavelengths in the range from 1200 to 2000 Å (Code & Welch 1979). This phenomenon is called UVX or UV upturn (cf. Figure 1). Observational evidence shows that UVX increases with stellar metallicity. Burstein et al. (1988) found that ETGs with bluer 1550-V colour have larger stellar velocity dispersion σ and higher absorption line index Mg_2 . Giant elliptical galaxies with large σ values have $[Mg/Fe]$ index higher than most metal rich stars in the solar neighbourhood (Worthey, Faber & González 1992). The work of Boselli et al. (2005) and Donas et al. (2007) reinforces the conclusion of Burstein et al. (1988) that metallicity is a fundamental parameter, and that the stronger cases of UVX occur in massive metal rich ($Z > Z_{\odot}$) ETGs.

The launch of the Galaxy Evolution Explorer (*GALEX*) satellite revolutionised the study of the UV emission of galaxies (Martin et al. 2005). Combined *GALEX* and Sloan Digital Sky Survey (*SDSS*, Stoughton et al. 2002) observations have revealed that a substantial fraction ($\sim 30\%$) of ETGs exhibit strong NUV and FUV emission, consistent with residual star formation (Kaviraj et al. 2007;

Schawinski et al. 2007), and that only a small percentage ($\sim 5\%$) of ETGs shows the classical UVX (Yi et al. 2005, 2011).

Using *GALEX* colours combined with SAURON spectroscopy, and rejecting galaxies with recent star formation, Bureau et al. (2011) found that galaxies with bluer FUV-V colour have stronger *Mgb* and lower *H β* absorption. This result suggests that galaxies with bluer FUV-V are older or have higher metallicity, or both. A similar conclusion was reached by Smith, Lucey & Carter (2012) studying a sample of 150 red and passive Coma cluster galaxies with spectroscopic age and estimated element abundances determinations. They also found a strong correlation of FUV-NUV colour with age and metallicity.

Nowadays, the favoured candidate sources for the UVX are extreme horizontal branch (EHB) stars and their descendants (Greggio & Renzini 1990; Rosenfield et al. 2012). EHB stars are low-luminosity core He-burning stars with temperatures reaching up to 23000 K and lifetime $\sim 10^8$ yr. Hence, they are difficult to observe, but they contribute considerably in the UV region of the spectrum, especially in galaxies dominated by old stellar populations like ETGs. EHB stars are observed in galactic globular and open clusters (e.g. NGC2808, ω Cen, NGC 6791) and among field stars (Catelan 2009). The dwarf elliptical galaxy M32 (Brown et al. 2000) is the only extragalactic stellar system

* E-mail: fhernandez@cida.gob.ve

with resolved EHBs. Rosenfield et al. (2012) observed over 4000 old hot stars in the bulge of M31 and classified them into three classes: Post-AGB (P-AGB) stars, Post-Early AGB (PE-AGB) stars, and AGB-manquè stars. They conclude that the stars detected contribute only about 2% of the total flux in the WFC3/UVIS F275W filter, and suggest that the missing stars responsible for this emission are most likely faint EHB stars. This result indicates that the stars responsible for the UVX have not yet been detected with certainty.

A number of competing mechanisms have been proposed to explain the origin of EHB stars. Greggio & Renzini (1990) argue for a single star origin. The large amount of mass loss during the RGB phase of high metallicity stars leads to a hot, low envelope mass EHB star. Once the star leaves the HB, depending on the envelope mass and the metallicity, the EHB star may skip the AGB phase and evolve through a more luminous post-EHB phase: either P-AGB, or PE-AGB, or AGB-manquè. The presence of EHB stars and the strength of the UVX should then depend strongly on the age and metallicity of the stellar population. On the other hand, Han et al. (2002, 2003) propose that EHB stars result from the interaction of binary stars through one of three possible channels: common-envelope (CE) ejection, stable Roche lobe overflow (RLOF), or two Helium white dwarf merger (2HeWD). In this scenario, the strength of the UV upturn should depend weakly on the age and metallicity of the stellar population (Han, Podsiadlowski & Lynas-Gray 2007, 2010).

One motivation of the work by Smith et al. (2012) was to distinguish between the single or binary star origin of EHB stars using the UVX in passive ETGs. They favour the metal rich single star origin of these stars. The main argument against the binary star origin of EHB is the expectation that, at least to some level, the UVX should be a universal phenomenon observable in all ETGs, uncorrelated with the age and metallicity of the stellar population.

In this paper we explore to what extent stellar population synthesis models that include the formation of EHB stars through binary star interactions can explain the UVX in ETGs. In Hernández-Pérez & Bruzual (2013) (hereafter, HB13) we presented such a model and showed that it can explain successfully the observed colour-magnitude diagram of the metal-rich galactic open cluster NGC 6791. Confirmed EHB stars are present in this cluster. If we consider the stellar population in this cluster archetypal of the stellar population in ETGs that show UVX, then our model should be adequate to study the UV upturn in ETGs. In § 2 we assemble a sample of ETGs with UV and optical detections, and use the UV r colour-colour plane to classify these galaxies as either star forming, UV weak, or UVX. In § 3 we review the most important aspects and parameters of the HB13 models. The predicted UV-optical colours from these models are compared with the data in § 4. The results are discussed in § 5 and the conclusions are presented in § 6.

2 THE ETG SAMPLE

To study the UVX phenomenon in ETGs using the HB13 models we must build a sample of galaxies observed both in the UV and optical ranges. The *SDSS* and the *GALEX*

Medium Imaging Survey (GALEX-MIS) overlap over 1000 square degrees in the sky and contain a considerable number of objects in common. We use the following *SDSS* pipeline parameters to select ETG candidates from the *SDSS-DR8*¹ (Aihara et al. 2011a,b), which will then be matched to their *GALEX* counterparts.

- (i) $fracDev_g > 0.95$: rejects spiral arms and blue disks,
- (ii) $fracDev_r > 0.95$: selects objects that follow the $r^{1/4}$ law in the r band, and
- (iii) $fracDev_i > 0.95$: reinforces constrain (i)

These purely morphological criteria, with no assumption on colours or spectral energy distributions, were proposed by Kaviraj et al. (2007) and Schawinski et al. (2007) in order to include more genuine ETGs than, e.g., Bernardi et al. (2003). According to Kaviraj et al. (2007) and Schawinski et al. (2007) these criteria are fulfilled by ETGs brighter than $r = 16$. Selecting galaxies with $r \leq 16$ guarantees the completeness of the sample at the top of the red region ($NUV-r = 6.2$) defined by Yi et al. (2005). Additionally, we keep only those galaxies with good spectral quality ($S/N > 10$) and redshift $z < 0.1$. This limits the volume of the sample to the local universe, so that no cosmological considerations enter this study. We end up with a sample of 64142 *SDSS* local ETGs brighter than $r = 16$.

Now we proceed to find the *SDSS* ETG candidates present in the *GALEX* sample as well. The *GALEX-MIS* sixth data release (GR6) contains 1500 s single orbit exposures in the NUV band (near-ultraviolet, centred at 2271 Å) and the FUV band (far-ultraviolet, centred at 1528 Å). The AB-system limiting magnitude in these bands is 22.7 and 22.6, respectively (Morrissey et al. 2005). Budavári et al. (2009) applied Bayesian statistics to achieve a cross-matched catalog using a large amount of data from the *SDSS* and the *GALEX* surveys. They found that a search radius of 4 arc sec in the $(\alpha, \delta)^2$ source position is acceptable to match objects present in both surveys. We adopt their value in this study. By means of SQL queries to *GALEX* CasJobs, we selected 5771 *SDSS* ETGs detected in both the FUV and the NUV bands with $S/N \gtrsim 3$ in the NUV.

Active Galactic Nuclei (AGN) are present in our sample. AGN in the local universe host preferentially massive elliptical galaxies (Kauffmann et al. 2003). Type I AGN (Quasars) are easily removed from the sample using the tag included in the *SDSS* pipeline. To remove type II AGN (Seyfert and LINERs) and star bursts (SB) we use the line ratios $[OIII]/H_\beta$ and $[NII]/H_\alpha$, as proposed by Kauffmann et al. (2003), in a modified version of the BPT diagram (Baldwin, Phillips & Terlevich 1981):

- (i) Seyfert: $[NII]/H_\alpha > 0.6$ and $[OIII]/H_\beta > 3$,
- (ii) LINER: $[NII]/H_\alpha > 0.6$ and $[OIII]/H_\beta < 3$, and
- (iii) SB: $\log([OIII]/H_\beta) > 0.61 / \{ \log([NII]/H_\alpha - 0.05) \} + 1.3$.

According to these rules, $\sim 26\%$ of the galaxies in our sample are AGN. This is consistent with the $\sim 25\%$ of type II AGN found by Kaviraj et al. (2007) in their ETG sample.

¹ The DR8 (the eighth *SDSS* data release) is complete to $r = 22.2$ mag. $fracDev_x$ is a structural parameter which indicates the fraction of the light of a galaxy that follows the de Vaucouleurs (1948) $r^{1/4}$ law in the x band. For the r band, $\lambda_{eff} = 6165$ Å.

² Right Ascension and Declination

Table 1. UV classification scheme (Yi et al. 2011).

Criterion	Description
$FUV-NUV < 0.9$	UV rising slope.
$NUV-r > 5.4$	Devoid of young massive stars.
$FUV-r < 6.6$	Strong FUV flux (UVX).

Even though the Kaviraj et al. (2007) and Schawinski et al. (2007) morphological classification excludes late-type galaxies, and the BPT method removes possible intruders, an important fraction of ETGs may have undergone recent star formation. Using the Bruzual & Charlot (2003) stellar population synthesis models (BC03 hereafter) computed for the Stelib (Le Borgne et al. 2003), Miles (Sánchez-Blázquez et al. 2006), and IndoUS (Valdes et al. 2004) stellar libraries over the range of typical ETG solar and super-solar metallicity, we find that for a simple stellar population (SSP) in the age range 5-10 Gyr, the equivalent width (EW) of $H\beta \lesssim 2.1 \text{ \AA}$. A similar result was found by Bureau et al. (2011). Discarding galaxies with $EW H\beta > 2.1 \text{ \AA}$, we end up with a catalogue of 3417 ETGs with both UV *GALEX* and optical *SDSS* photometry, and no signs of nuclear activity and/or important events of recent star formation. In § 4 we will use this sample to compare with the predictions of the HB13 models.

2.1 UV-classification scheme

The position of the 3417 ETGs in the (FUV-NUV) vs. (NUV-*r*) two colour diagram (UV r 2CD hereafter) is shown in Figure 1. The colours of the galaxies shown in the Figure have been corrected for Galactic foreground extinction using the Schlegel, Finkbeiner & Davis (1998) maps. We assume the UV extinction law from Wyder et al. (2005), and the Fukugita et al. (2004) formula for the *SDSS* *r* band. The galaxies in our sample are in the local universe ($z \lesssim 0.1$), therefore, evolutionary corrections are irrelevant. In Figure 1 the arrow indicates the typical *k*-correction vector determined by Yi et al. (2011). The length of this arrow is similar to the size of the dots representing galaxies, hence the *k*-correction is negligible.

The wide range of (FUV-NUV) and (NUV-*r*) colours covered by the ETGs in Figure 1 indicates that the relative amount of UV flux in these galaxies is far from uniform. This behaviour can be explained by the presence of either EHB stars, hot evolved stars, or young massive stars in different proportions in each galaxy. The slope of the UV spectrum is related to the temperature of the stars emitting in the UV. Yi et al. (2011) established a colour criterion to classify ETGs according to their UV spectral morphology, illustrated in Figure 1 and summarised in Table 1. $FUV-NUV = 0.9$ indicates a flat UV spectrum, whereas a bluer FUV-NUV corresponds to a steeper slope. Passively evolving ETGs have $NUV-r \geq 5.4$ and $FUV-r > 6.6$. The $NUV-r = 5.4$ line indicates the blue limit of the red sequence. UV strong ETGs obey the three conditions in Table 1.

As indicated in Figure 1, according to the Yi et al. (2011) UV classification criterion, $\sim 48\%$ of the galaxies in our sample of ETGs are classified as UV weak galaxies, \sim

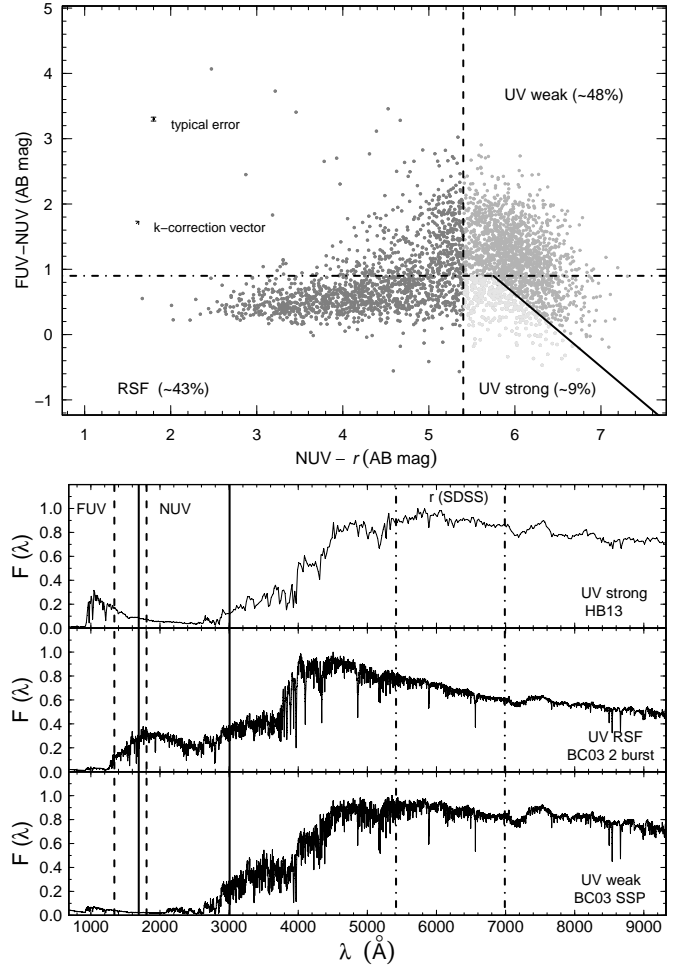


Figure 1. *Top:* UV r 2CD showing the 3417 galaxies classified as ETGs in § 2. Vertical dashed line: $NUV-r = 5.4$, horizontal dot dashed line: $FUV-NUV = 0.9$, and inclined solid line: $FUV-r = 6.6$ (see Table 1). Typical error bars and *k*-correction vector are plotted. The data has been corrected for Galactic extinction. Red and black dots represent UV strong (UVX) and UV weak ETGs, respectively. Blue dots correspond to ETGs with recent star formation. *Bottom:* Typical spectral energy distribution of UV strong (UVX), RSF and UV weak ETGs. The UVX spectrum was computed using the HB13 models. The BC03 models were used to compute the RSF and UV weak galaxy spectra. The wavelength range covered by the FUV, NUV, and *r* filters are indicated by the vertical lines.

43% as residual star forming (RSF) galaxies, and only $\sim 9\%$ as UV strong (or UVX) galaxies. These percentages are in good agreement with those found by Yi et al. (2011) only if galaxies detected in both the FUV and the NUV are considered, as we do in our sample³. Our models do not intend nor pretend to explain the percentage of galaxies seen in each region of Figure 1. UVX is present in about 20% of non RSF ETG's. It is likely that UVX is also present in a similar fraction of RSF galaxies, but is hidden by the UV emission of young massive main sequence stars present in these galax-

³ Our sample of ETG's will be made available to the interested reader. See Table 2

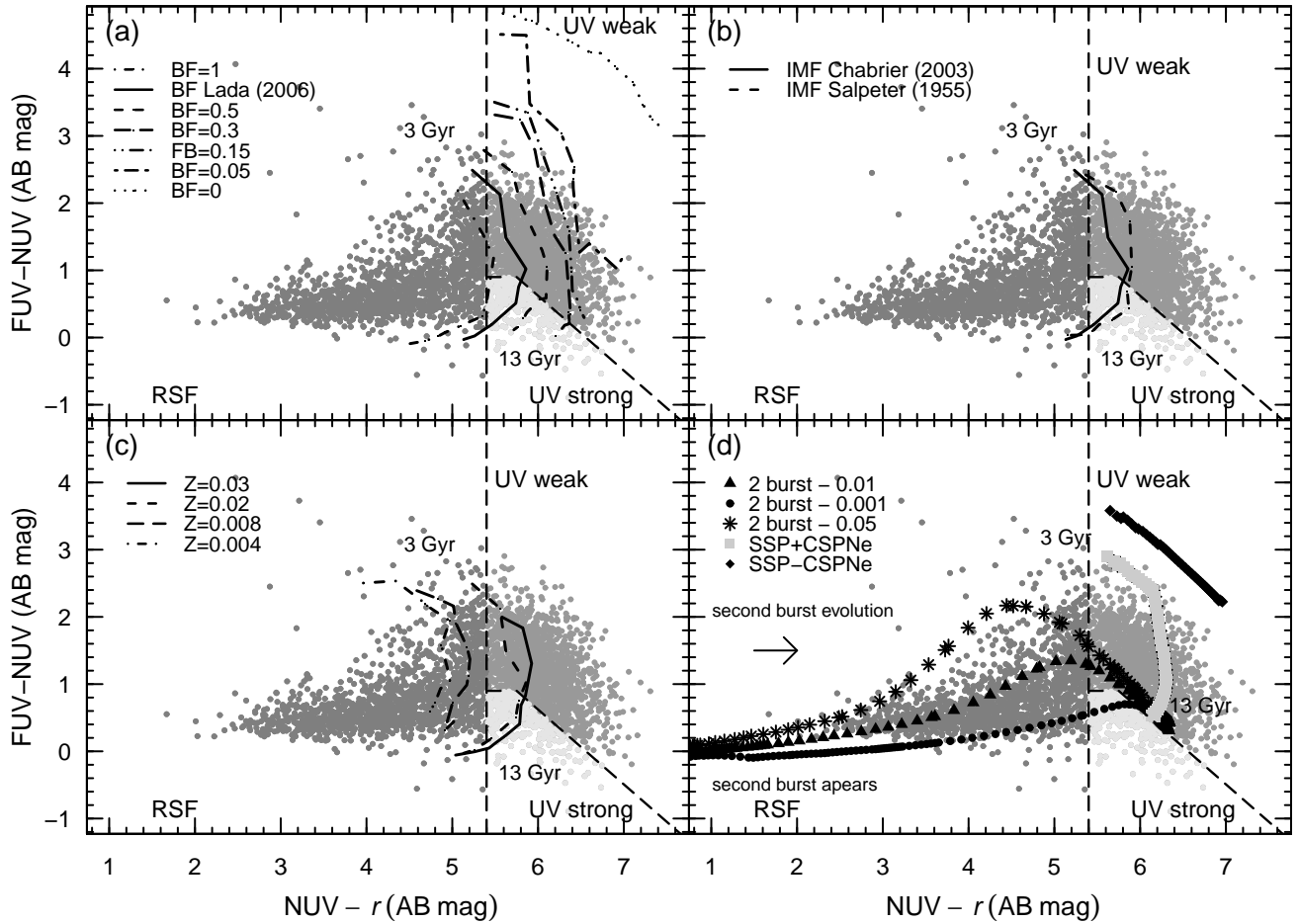


Figure 2. *a,b,c*: The lines show the colour evolution of various HB13 models in the UV r 2CD. Time varies from 3 Gyr at the red FUV-NUV end of the line to 13 Gyr, where models reach the region of UV strong (UVX) ETGs. (*a*) Colour evolution for different values of the fraction of binary stars (BF) as indicated in the figure. (*b*) Colour evolution for the Chabrier (2003) and Salpeter (1955) IMF models. (*c*) Colour evolution for models of different stellar metallicity Z , as indicated in the figure. (*d*) Colour evolution of standard BC03 models in which a second burst of star formation occurs when the stars formed in the first burst are 12 Gyr old. Different symbols represent bursts of different amplitude, indicated in the figure as the fraction of the total mass. These bursts add 0.1, 1, and 5% to the initial mass of the galaxy. When the second burst occurs the NUV- r colour changes drastically towards the blue, reaching the NUV- r < 3 RSF region in the UV r 2CD. As the massive stars in the second burst fade away, NUV- r becomes redder and the stellar population eventually recovers the colours it had before the second burst. The higher the amplitude of the second burst, the redder the FUV-NUV colour reached by the stellar population in the post burst era. For reference, a BC03 SSP model, including and excluding CSPNe, is also plotted.

ies. In the next section we discuss some scenarios that may explain why 80% of the ETG's avoid the UVX phenomenon.

3 SPS INCLUDING BINARY STARS

In HB13 we constructed a stellar population synthesis (SPS) model that includes interacting binary stars. We use the Hurley, Tout & Pols (2002) BSE public code to compute the evolutionary tracks of a population of binary pairs. The BSE code follows the evolution of the physical and orbital parameters of both members of a pair through all phases of stellar evolution from the ZAMS up to the remnant stage. The distributions of period, mass ratio, and the fraction of binary stars are carefully modelled to reproduce the observational trends as much as possible. The most relevant binary star interactions, including RLOF, CE, mass transfer, mass ac-

cretion, supernova kicks, and angular momentum loss are followed in the BSE code. The occurrence of one or more of these processes depends on the orbital and initial physical parameters of the pair. In the standard version of the BSE code, when the 2HeWD in a binary pair collide, the temperature of the merger product becomes too hot and the object is destroyed. In our version of the BSE code, we use the Han et al. (2002) conditions for He to ignite after the 2HeWD merger occurs. In this case, we assign physical parameters to the resulting EHB star using the BaSTI data set, based on evolutionary tracks computed with realistic stellar physics by Pietrinferni et al. (2004, 2006). Our code then includes EHB stars formed through one of these channels: RLOF, or CE, or 2HeWD merger.

In HB13 we used our model to explain successfully the observed colour-magnitude diagram of the metal-rich ($Z = 0.03$) galactic open cluster NGC 6791, which contains

a significant number of confirmed EHB stars, resulting in a synthetic spectrum with a strong UVX. If the stellar population in this cluster is archetypal of the stellar population present in UVX galaxies, then our model should be adequate to study the UV upturn in ETGs. See HB13 for details.

4 MODELLING THE UVX

4.1 Model parameters

Observational evidence shows that ETGs exhibit different degrees of UV emission (cf. Figure 1). In this section we examine the range of values covered by the UV colours and UVX as we vary the HB13 model input parameters. In these models the rate of EHB star formation is controlled by the following parameters: (a) Fraction of binary stars (BF), (b) Initial mass function (IMF), and (c) Stellar metallicity (Z). Unless stated otherwise, models discussed below represent SSPs computed for the Chabrier (2003) IMF, the Lada (2006) spectral type dependent BF, and the solar metallicity ($Z = 0.02$) Hurley et al. (2002) binary star evolutionary tracks. The IMF extends from 0.1 to 100 M_{\odot} .

Additionally, a binary pair is characterised by its orbital period (P), orbit eccentricity (e), and mass ratio ($q = M_2/M_1$). As in HB13 we assume that e and q are distributed uniformly, following Zhang et al. (2004, 2005), and Milone et al. (2012), respectively, and that P follows the Gaussian distribution (in $\log P$) found by Duquennoy & Mayor (1991), with $\overline{\log P} = 4.4$, and $\sigma_{\log P} = 2.3$, where P is measured in days. In the tests below the distributions of P , e , and q are kept fixed.

4.1.1 Binary Fraction

Since in the HB13 models all EHB stars are formed via binary star interactions, the resulting number of EHB stars depends on the value of BF characterising the population. To study the influence of BF on the UV colours of the model population, we computed HB13 models for the following values of BF: (a) BF=0, all stars are single; (b) BF=0.05, 5% of the stars are in binary systems; (c) BF=0.15, 15% of the stars are in binary systems; (d) BF=0.3, 30% of the stars are in binary systems; (e) BF=0.5, 50% of the stars are in binary systems; (f) BF=Lada, BF depends on spectral type following Lada (2006); and (g) BF=1, all stars are in binary systems. The predicted colour evolution is shown by the different lines in Figure 2a. Models with $\text{BF} \geq 0.30$ reproduce the observed colours of ETGs in both the UV-weak and UV-strong regions of the UVr2CD. It is significant that a minimum BF is required to reproduce these colours. The colours of ETGs catalogued as RSF cannot be reproduced, not even for BF = 1.

Dorman et al. (1995) developed a spectral synthesis model that includes all phases of single star evolution, from the ZAMS to the white dwarf phase. They find that for the bulk of ETGs $\sim 5\%$ of the stars on the HB are EHB stars, whereas for UVX galaxies this fraction reaches $\sim 20\%$, which is not far from our results. Kalirai et al. (2007) determined that at least 40% of the evolved stars in NGC 6791 have lost enough mass on the RGB phase to avoid the helium flash, and Bedin et al. (2008) established that in NGC 6791 BF \sim

25-35%. These results suggest that BF is not the same in all stellar systems.

4.1.2 Initial Mass Function

The rate of production of atypical stars by interacting binary pairs, like EHB stars or blue stragglers, depends on the frequency of progenitors in the appropriate mass range, which is determined by the IMF. The probability to form a binary system that will evolve into two HeWD will be higher for those IMFs richer in their progenitors. Thus, despite the narrow mass range (0.4-0.65 M_{\odot}) of the progenitors of EHB stars formed through the 2HeWD merger channel, we expect a slight dependence of the number of these stars on the IMF.

Figure 2b shows the colour evolution of models computed with the Salpeter (1955) and the Chabrier (2003) IMFs. For both IMF's the models reproduce the range of colours of passively evolving ETGs in the UV weak and UV strong regions of the UVr2CD. The Chabrier IMF model colours are bluer in NUV- r . The frequency of EHB progenitors is higher for the Chabrier than for the Salpeter IMF. The Salpeter IMF yields a higher number of stars with mass below 1 M_{\odot} than the Chabrier IMF.

4.1.3 Metallicity

The number of EHB formed by binary interactions should not depend on stellar metallicity, but only on the distribution of the orbital parameters of the pairs (Han et al. 2007). Smith et al. (2012) argue that the influence of metallicity on these models is neither completely addressed nor fully evaluated, because even if the formation of the binary systems does not depend on metallicity, the subsequent evolution of the EHB star does. The physical parameters of EHB stars in our models are derived from the BaSTI data set, which does include the metallicity dependence. Figure 2c shows the colour evolution of models computed for $Z = 0.004, 0.008, 0.02$, and 0.03 . As expected, high Z models ($Z = 0.03$ and 0.02) reproduce well the colours of UV weak and UV strong ETGs. The $Z = 0.03$ model is slightly bluer than the $Z = 0.02$ model. Thus, the HB13 models predict a correlation between the strength of UVX and metallicity. The Hurley et al. (2002) code does not allow to compute tracks for $Z > 0.03$. Subsolar models ($Z = 0.008$ and 0.004) are bluer in (NUV- r) because of the presence of blue HB stars resulting from the evolution of single stars.

4.2 Two bursts of star formation

Although most of the ETGs in our sample are located in the UV weak and UV strong regions of the UVr2CD, approximately 43% of the galaxies are located in the RSF region. Kaviraj et al. (2007), Schawinski et al. (2007), Kaviraj et al. (2008), and Kaviraj (2010) report observational evidence that the blue NUV- r colour of these galaxies is due to residual star formation within the last 1 Gyr. In particular, Kaviraj (2010) concludes that ETGs with blue UV colours are morphologically perturbed and that these colours are driven by merger-induced star formation within the last 3 Gyr.

Galaxies with NUV- $r < 5.4$ can not be explained in

terms of the HB13 SSP models discussed in the previous subsections and shown in Figures 2a,b,c. HB13 models for arbitrary star formation histories are not yet available. To understand the colours of the bluest galaxies in Figure 2, we use the standard BC03 models. The BC03 models do not include binary stars, and lack the EHB star contribution present in the HB13 models. However, the massive main sequence O-B stars formed in a recent burst of star formation will outshine in the UV the contribution of the EHB formed in the initial burst. In Figure 2d we show the path followed in the UV r 2CD by models in which a second burst of star formation occurs when the stars formed in the first burst are 12 Gyr old. Different symbols represent bursts of different amplitude, as indicated in the figure.

The standard BC03 SSP model is also shown in Figure 2d. The central stars of planetary nebulae (CSPNe) included in this model are responsible of the UV flux seen at late ages. For comparison we include an SSP models in which CSPNe have been suppressed. This latter model resembles the HB13 model for BF = 0.

The lowest amplitude burst (0.1%) traverses the UV strong region in Figure 2d on its way to bluer colours. However, the time spent by this model in the UV strong region is quite short, less than 0.15 Gyr. The effects of this burst on the integrated spectrum last for no longer than 0.7 Gyr. Therefore, the probability that all ETGs catalogued as UV strong have suffered a recent (in the last ~ 0.55 -0.7 Gyr) and low amplitude ($\sim 0.1\%$ of the total mass) burst is small. Additionally, studies of resolved stars in the bulge of M31 (Rosenfield et al. 2012) and in M32 (Brown et al. 2000), do not show the presence of MS stars.

5 DISCUSSION

The principal aim of this study is to fill the gap between the classical models (single star scenario) to explain the UVX phenomenon (e.g. Yi, Demarque & Oemler 1997) and models that include interacting binaries (e.g. Han et al. 2010). In both type of models the UVX is produced by EHB stars (He burning stars with $T_{eff} > 23000$ K). EHB stars are considered the most likely source of the UVX despite the fact that they are not resolved in extragalactic objects (Brown et al. 1997, 2008; Rosenfield et al. 2012). In the classical model, EHBs are the product of the evolution of high Z or He enhanced low mass single stars. In the interacting binary models EHB stars are formed via binary interactions through mass transfer, collisions, or mergers. Therefore, the two models make different predictions for the evolution of the UVX in ETGs. In the classical model, the intensity of the UV flux increases with the age of the stellar population because low mass stars have less gravitationally bound lower mass envelopes, which are easier to lose through mass loss during the RGB evolution, producing blue HB stars. Since the mass loss rate increases with Z , in this model the UVX is expected to increase with the metallicity of the stellar population. Carter et al. (2011) and Smith et al. (2012) find such a correlation of UVX with age and metallicity, and conclude that the most probable source of the UVX is evolved low mass stars.

On the other hand, from interacting binary models we do not expect a relation between the UVX and age or Z

(Han et al. 2002). Han et al. (2007) show that the FUV- r colour is almost constant for age between 3 and 12 Gyr. In principle, in these models the UVX is not related to Z because the formation channel of EHBs depends only on the orbital parameters of the binary pairs. But, as indicated in § 1, once the EHB star is formed, its position and subsequent evolution in the HR diagram *does* depend on Z . The HB13 model predicts that the ETGs inside the UV strong region are the oldest (Figure 2). This result is related to the use of the Pietrinferni et al. (2004, 2006) evolutionary tracks to assign the physical properties to EHBs formed as a result of a 2HeWD merger. These tracks allow for a narrow range of mass for the EHB stars, from 0.49 to 0.53 M_{\odot} . Since the mass of the EHB star is the sum of the mass of the two merging WDs, the probability of producing an EHB star in the indicated mass range via the 2HeWD merger channel increases with time. As shown in Figures 2a,b,c, in the HB13 models the UVX phenomenon appears in old stellar populations ($\gtrsim 7$ Gyr). Figure 2c shows a weak correlation between Z and the UV colours inside the UV strong region of the UV r 2CD. The $Z = 0.03$ model is slightly bluer than the $Z = 0.02$ model in the UV strong region. A more detailed treatment of the evolution in the post-EHB phases would help establishing the reality of these two correlations.

It is important to remark that the HB13 models reproduce all ETGs in the sample catalogued as UV weak or UV strong for some choice of BF, Z , or the IMF. The distribution of these parameters, and others like orbital period and mass ratio, and its temporal evolution and dependence with environment remain an unresolved puzzle.

6 SUMMARY AND CONCLUSIONS

We use the HB13 SPS models, which include the evolution of interacting binary stars, as a tool to study the UVX phenomenon observed in ETGs. First we build a sample of ETGs with observed optical (*SDSS*-DR8) and UV (*GALEX*-GR6) photometry. Following Yi et al. (2011), we classify the ETGs in our sample according to their position in the UV r 2CD as UV weak (galaxies in the red sequence), UV strong (galaxies with UVX), and RSF (galaxies that have experienced recent episodes of star formation). Then, we compare the UV colours of the sample galaxies with the colour evolution lines in this plane predicted by the HB13 models, varying, one at a time, the fraction BF of binary stars, the IMF, and the stellar metallicity Z .

In view of the results discussed in § 4, we conclude that:

- Of all parameters tested, the UVX is most sensitive to BF. Varying BF it is possible to reproduce the UV colours of almost all the ETGs in the UV weak and UV strong regions of the UV r 2CD, as long as BF is above a threshold value of ~ 0.15 .
- Although the Chabrier (2003) IMF model is slightly bluer in NUV- r than the Salpeter (1955) IMF model, both models are in good agreement with the observed colours of UV weak and UV strong ETGs.
- Higher metallicity models ($Z = 0.02$ and $Z = 0.03$) reproduce the colours of UV weak and UV strong galaxies better than low Z models. The $Z = 0.03$ model is slightly bluer than the $Z = 0.02$ model in the UV strong region. This behaviour seems indicative of a weak relationship between

UVX and Z . The HB stars present in the low Z models move the integrated NUV- r colour into the RSF region.

- The colours of the ETGs in the RSF region of the UV r 2CD cannot be understood in terms of the HB13 SSP models. These colours are well reproduced by standard BC03 models, which lack binary stars, when a second burst of star formation is added to the old stellar population. A burst strength of $\sim 5\%$ of the total mass of the stellar system suffices to explain the colours of the RSF galaxies.

- The largest values of UVX occur at the oldest age in the model population (13 Gyr).

We would like to stress our last conclusion because the lack of a relation between UVX and age and Z in models that assume that EHB stars result from binary interactions has been taken as a weakness of these models. Despite Smith et al. (2012) remark that these models cannot account naturally for the observed trends of UVX with age and metallicity, we have shown that the HB13 models predict a clear dependence of UVX with age, and to a lesser extent with Z .

When the tools to compute the evolution of binary pairs are improved, especially a better coverage of the tracks in the (Y, Z) plane, and an adequate treatment of the post-EHB phases of stellar evolution, it will be possible to explore these trends in depth. In real galaxies EHB stars may form both from single stars and from binary pairs.

ACKNOWLEDGMENTS

We are very grateful to the referee, Phil Rosenfield, who provided useful comments and suggestions that helped to improve this paper. FHP acknowledges the hospitality of the UNAM Centro de Radioastronomía y Astrofísica during the last stages of this investigation. FHP acknowledges support from CIDA during her PhD thesis work partially reported in this paper. GB acknowledges support for this work from the National Autonomous University of México, through grants IA102311 and IB102212-RR182212. This work has made use of the BaSTI web tools.

REFERENCES

- Aihara H., et al. 2011a, ApJ, 193, 29
 Aihara H., et al. 2011b, ApJ, 195, 26
 Baldwin J.A., Phillips M.M., & Terlevich R. 1981, PASP, 93, 5
 Bedin L., Salaris M., Piotto G., Cassisi S., Milone A., Anderson J., King I., 2008, ApJ, 679, L29
 Bernardi M., et al. 2003, AJ, 125, 1817
 Boselli A., et al. 2005, ApJ, 629, L29
 Brown T.M., et al. 1997, ApJ, 482, 685
 Brown T.M., et al. 2000, ApJ, 532, 308
 Brown, T.M., et al. 2008, ApJ, 682, 319
 Bruzual G., Charlot S., 2003, MNRAS, 344, 1000 (BC03)
 Budavári T., et al. 2009, ApJ, 694, 1281
 Bureau M., et al. 2011, MNRAS, 414, 1887
 Burstein D., et al. 1988, ApJ, 328, 440
 Carter D., et al. 2011, MNRAS, 414, 3410
 Catelan M., 2009, Ap&SS, 320, 261
 Chabrier, G. 2003, PASP. 115, 763
 Code A.D. & Welch G.A., 1979, ApJ, 228, 95
 de Vaucouleurs G. 1948, Annales d’Astrophysique, 11, 247
 Donas J., et al. 2007, ApJS, 173, 597
 Dorman, B., O’Connell, R. W., & Rood, R. T. 1995, ApJ, 442, 105
 Duquenois A. & Mayor M. 1991, A&A, 248, 485
 Fukugita, M., et al. 2004, AJ, 127, 3155
 Greggio L. & Renzini A., 1990, ApJ, 364, 35
 Han Z., et al. 2002, MNRAS, 336, 449
 Han Z., et al. 2003, MNRAS, 341, 669.
 Han Z., Podsiadlowski P., & Lynas-Gray A., 2007, MNRAS, 380, 1098
 Han Z., Podsiadlowski P., & Lynas-Gray A., 2010, Ap&SS, 329, 41
 Hernández-Pérez F. & Bruzual G., 2013, MNRAS, 431, 2612 (HB13)
 Hurley J., Tout C., & Pols O., 2002, MNRAS, 329, 897
 Kalirai J. S., Bergeron P., Hansen B. M. S., Kelson D., Reitzel D., Rich R. M., Richer H. B. 2007, ApJ, 671, 748
 Kauffmann G., et al. 2003, MNRAS, 346, 1055
 Kaviraj S. 2010, MNRAS, 408, 170
 Kaviraj S., et al. 2007, ApJS, 173, 619
 Kaviraj S., et al. 2008, MNRAS, 388, 67
 Lada, C.J. 2006, ApJL, 640, L63
 Le Borgne, J.-F., et al. 2003, A&A, 402, 433
 Martin D.C., et al. 2005, ApJ, 619, L1
 Milone A.P., et al. 2012, A&A, 540, A16
 Morrissey P., et al. 2005, ApJ, 619, L7
 Pietrinferni A., et al. 2004, ApJ, 612, 168
 Pietrinferni A., et al. 2006, ApJ, 642, 797
 Rosenfield P. et al., 2012, ApJ, 755, 131
 Salpeter, E.E. 1955, ApJ, 121, 161
 Sánchez-Blázquez, P. et al. 2006, MNRAS, 371, 703
 Schawinski K., et al. 2007, ApJS, 173, 512
 Schlegel, D.J., Finkbeiner, D.P., & Davis, M. 1998, ApJ, 500, 525
 Smith R., Lucey J., & Carter D., 2012, MNRAS, 421, 2982
 Stoughton C., et al. 2002, AJ, 123, 485
 Valdes, F., et al. 2004, ApJS, 152, 251
 Worthey, G., Faber, S.M., & González, J.J. 1992, ApJ, 398, 69
 Wyder, T.K., et al. 2005, ApJL, 619, L15
 Yi S.K., Demarque P. & Oemler, A., Jr. 1997, ApJ, 486, 201
 Yi S.K., et al. 2005, ApJ, 619, L111
 Yi S.K., et al. 2011, ApJS, 195, 22
 Zhang F., et al. 2004, A&A, 415, 117
 Zhang F., et al. 2005, MNRAS, 357, 1088

This paper has been typeset from a \TeX / \LaTeX file prepared by the author.

Table 2. Sample of ETGs. The full catalogue is available online.

petroMag_u	petroMag_g	petroMag_i	ra_sdss	dec_sdss	l	b	petroMag_r	Mr	Mi
18.29143	16.35660	14.97087	46.02846908569	0.40545412898	177.58947753906	-47.87882995605	15.42630958557	-21.209989414430000	-21.665429133300783
19.46463	17.59273	16.16457	46.21551513672	0.74301409721	177.41708374023	-47.51077270508	16.63254928589	-20.491451714110000	-20.959430549316405
18.24109	16.74386	15.52379	46.26059341431	0.62891566753	177.58561706543	-47.55664062500	15.93988037109	-21.644618628910003	-22.060709359130860
18.14983	16.71730	15.52285	46.47204589844	0.69790321589	177.72631835938	-47.35560989380	15.73655986786	-21.576341132139994	-21.790050543212892
18.00752	16.21822	14.80156	49.79270553589	0.98124957085	180.64111328125	-44.70737457275	15.27602005005	-21.179080949950000	-21.653541013183590
18.95059	17.22444	16.04347	50.04067993164	0.38022595644	181.51036071777	-44.91334915161	16.46379089355	-20.047607106450000	-20.467928315429690
17.60561	15.74392	14.37742	50.77199935913	0.35427513719	182.20343017578	-44.37268066406	14.83160972595	-21.574388274049994	-22.028578229980468
17.61876	16.08453	15.09293	51.70888137817	0.19859315455	183.20352172852	-43.75176239014	15.43039035797	-19.516310642030000	-19.853771049804685
17.99723	16.39799	14.99610	124.38243103027	6.10155057907	217.36697387695	21.90885353088	15.42607021332	-22.277630786680003	-21.570428773193360
18.55027	17.08896	15.89254	124.77439880371	6.53160905838	217.14175415039	22.45036315918	16.25268936157	-20.851508638429998	-20.851669450683595

Table 2. (Continued)

Mg	Mu	log10([NII]/Ha)	log10([OIII]/Hb)	ObjID_GALEX	ra_galex	dec_galex	nuv_mag	nuv_magerr	fuv_mag
-20.279699133300780	-18.344869133300783	-0.2091223900	-0.2043416600	3785488929565709817	46.028564	0.40498918	21.2482590	0.09381471570	22.6063080
-19.531270549316407	-17.659370549316407	0.0326513015	0.3268755100	3785488929565713254	46.215191	0.74286103	22.4296970	0.17540295000	23.2013070
-20.840639359130858	-19.343409359130860	-0.1805296400	0.0451106206	3785488929565712010	46.260437	0.62884051	19.6889100	0.02934143130	20.1846500
-20.595600543212890	-19.163070543212890	-0.2740299700	0.0775291473	3785488929565712479	46.471992	0.69746453	22.0325220	0.18447484000	23.5201870
-20.236881013183595	-18.447581013183594	-0.0645105466	0.1968973300	3786825935705089048	49.793007	0.98167664	20.9321560	0.15248564000	22.9935910
-19.286958315429686	-17.560808315429690	0.0252749734	0.0932619199	3786825935705084364	50.040009	0.37958860	19.9982170	0.05102190750	20.1983930
-20.662078229980470	-18.800388229980470	-0.0580598488	0.2722403100	3786755566960910813	50.772118	0.35446551	21.4960670	0.09262551370	22.6834660
-18.862171049804687	-17.327941049804686	-0.4772084700	-0.0895130560	3786720382588820183	51.709015	0.19873226	19.1738950	0.02219730240	19.8439540
-20.157218773193360	-18.596798773193360	0.1089163700	0.2294356100	3781055698682513729	53.574120	1.08439530	20.5764810	0.09053609520	21.1153790
-19.617089450683594	-17.622869450683595	-0.1380410500	0.2712974500	2883924579161478888	122.724420	6.77663950	20.8848510	0.10049001000	21.2323720

Table 2. (Continued)

fuv_magerr	NUV-r	FUV-r	FUV-NUV	FUV-i	NUV-i	objid_SDSS	specobjid
0.20705687000	5.8219494144300015	7.1799984144299990	1.3580489999999976	7.6354379999999990	6.2773890000000010	1237666301090595021	462885629684901888
0.35801402000	5.7971477141100000	6.5687577141099990	0.7716099999999990	7.0367369999999990	6.2651270000000000	1237666301627531441	799479405649881088
0.05326829850	3.7490296289100000	4.2447696289100010	0.4957400000000014	4.6608600000000010	4.1651200000000000	1237666301627531485	462894425777924096
0.52031946000	6.2959621321400000	7.7836271321399995	1.4876649999999998	7.9973370000000000	6.5096720000000000	1237666301627662490	463962883600967680
0.33395603000	5.6561359499499990	7.7175709499499980	2.0614349999999995	8.1920309999999980	6.1305959999999990	1237660241924194498	465120938703218688
0.06772778180	3.5344261064499990	3.7346021064499980	0.2001759999999990	4.1549230000000000	3.9547470000000010	1237666301092364510	465137156499728384
0.22112644000	6.6644572740499990	7.8518562740499980	1.1873989999999992	8.3060459999999980	7.1186469999999990	1237666301092692103	465171241360189440
0.04076994210	3.7435046420300020	4.4135636420300010	0.6700589999999984	4.7510239999999990	4.0809650000000010	1237663238739656839	466254534721693696
0.16861857000	5.0821410570700000	5.6210390570700000	0.5388979999999997	6.0919090000000010	5.5530110000000015	1237666302167613543	467373561154136064
0.12498153000	4.2160010549300000	4.5635220549300010	0.3475210000000004	4.9580420000000025	4.6105210000000020	1237661069236306358	1977119320752285696

Table 2. (Continued)

distMod	oiii_5007_reqw_2	oiii_5007_reqw_err	oiii_5007_flux_2	h_beta_reqw_2	h_beta_reqw_err	h_beta_flux_2	h_beta_flux_err	h_alpha_reqw_2	h_alpha_reqw_err
36.63630	1.11812600	0.1359332	14.33500	1.46240500	0.1334203	22.94771	9.462569	1.09284200	0.1165095
37.12400	-0.48105400	0.2117711	35.98407	1.37063700	0.2013691	16.95254	5.472645	-0.40364370	0.1744546
37.58450	-1.95989200	0.1999664	98.45863	-0.06592561	0.1905727	88.74485	5.497423	-10.08683000	0.1965194
37.31290	-0.32448870	0.2222320	24.08385	1.09846800	0.2139954	20.14637	5.081953	-0.17616400	0.1559426
36.45510	0.25660710	0.1449615	46.01131	1.44939000	0.1365565	29.23932	5.750356	0.66609720	0.1089979
36.51140	-0.01665873	0.2373855	17.76559	1.32882300	0.2316568	14.33236	3.651183	0.02611245	0.1616823
36.40600	0.38211290	0.1338232	48.29372	1.59029600	0.1295062	25.80182	6.596438	0.40637690	0.1111791
34.94670	-2.27055000	0.1090620	139.61810	1.02019500	0.1070480	171.57530	3.038154	-12.40400000	0.1168257
36.59390	-0.29583250	0.1650213	50.13787	1.09070300	0.1623713	29.56176	5.088054	-0.38688100	0.1317513
37.12600	-0.35881360	0.2922065	16.21037	1.46930500	0.2784692	8.67952	2.630958	-0.86980680	0.2085919

Table 2. Continued

h_alpha_flux_2	h_alpha_flux_err	nii_6584_reqw_2	nii_6584_reqw_err	nii_6584_flux_2	nii_6584_flux_err
24.26414	13.235710	0.0240101	0.1269430	14.99141	13.059910
65.49400	6.923422	-2.4672820	0.1681761	70.60783	5.207277
458.55660	8.598775	-7.6029160	0.1847260	302.59610	7.355111
48.97443	5.538928	-0.9081378	0.1582255	26.05790	4.541668
54.48049	6.518898	-0.8754932	0.1202214	46.96026	5.968427
37.60296	3.815626	-1.7129330	0.1647673	39.85630	3.507146
82.20546	8.495528	-1.0213470	0.1165855	71.91853	7.682998
670.11820	4.557004	-4.8004970	0.0900986	223.32790	2.795492
94.25098	6.266301	-2.7130420	0.1379573	121.11620	5.341981
43.83486	3.237773	-1.8116770	0.2014738	31.89911	3.026775